

IMECE2022-94882

**NONLINEAR ELECTRO-MECHANICAL IMPEDANCE SPECTROSCOPY FOR
COMPREHENSIVE MONITORING OF CARBON FIBER REINFORCED COMPOSITE
LAMINATES**

Runye Lu

University of Michigan-Shanghai Jiao Tong
University Joint Institute, Shanghai Jiao Tong
University, Shanghai, China

Yanfeng Shen

University of Michigan-Shanghai Jiao Tong
University Joint Institute, Shanghai Jiao Tong
University, Shanghai, China;
Shanghai Key Laboratory for Digital
Maintenance of Buildings and Infrastructure,
Shanghai, China

ABSTRACT

This paper presents a Nonlinear Electromechanical Impedance Spectroscopy (NEMIS) methodology for the comprehensive monitoring of carbon fiber reinforced composite (CFRC) laminates. This method can obtain structural impedance spectra and capture nonlinear ultrasonic features for damage detection, combining the merits of the conventional EMIS and the nonlinear ultrasonic techniques. A comparative illustration between the conventional EMIS and NEMIS is presented. Various damage types and damage mechanisms of CFRC laminates are reviewed. Numerical investigation on a reduced-order 1-D Contact Acoustic Nonlinearity (CAN) model are conducted to demonstrate the chirp-induced nonlinear features. Furthermore, a finite element (FE) model is established to verify the feasibility of the NEMIS for damage detection. The macro-scale damage types are modeled by the changes of material properties, while the incipient damage like delamination is simulated by setting the contact interfacing condition between the laminate debonding areas. Correspondingly, the chirp-based impedance spectra are employed to detect the macro-scale damage via the deviation of resonance peaks, while the nonlinear features, such as higher harmonics and wave modulation are utilized to monitor the delamination. Two damage indices are developed to quantify the severity of both the macro and incipient damage. This paper finishes with conclusion and suggestions for future work.

Keywords: electro-mechanical impedance spectroscopy; nonlinear ultrasonics; carbon fiber reinforced composite; structural health monitoring; delamination

1. INTRODUCTION

Carbon fiber reinforced composite (CFRC) laminates, by virtue of their high strength to weight ratio, strong corrosion

resistance, and excellent stiffness, have been pervasively applied in various industrial fields, including aviation, energy, marine, sports, and civil engineering [1-3]. Nonetheless, CFRC laminates are susceptible to complex external invasions, such as impact, moisture, thermal change, and cyclic loadings, which can lead to damage in CFRC materials and finally cause catastrophic consequences [4]. Structural Health Monitoring (SHM) and Nondestructive Evaluation (NDE) of CFRC laminates, hence, has aroused tremendous interests in both academia and industry.

CFRC laminates may suffer manufacturing defects and in-service damage, or become damaged due to inappropriate handling and installation [4]. Since CFRC consists of two components, namely the carbon fiber and the matrix, the damage mechanism is usually complicated [5]. Regarding manufacturing defects, including fiber waviness [6], voids [7], adhesion problem of interfaces, etc., they can result in a reduction of material properties or become an inducement for further damage. Handling and installation damage, can be attributed to accidental impacts [8-10] during transportation and inappropriate installation operation like hole-drilling [11, 12]. In particular, in-service damage is dominating since the working conditions for CFRC laminates are usually harsh and severe due to their high-end applications. The materials can be exposed to extreme temperature [13], moisture [14], intensive collision, and long-term cyclic loadings, resulting in delamination, fiber and matrix cracking [15], and fatigue damage.

It is acknowledged that CFRC possesses relatively low strength and stiffness in the transverse direction to fiber orientation, rendering the low resistance to impacts [10]. Therefore, among the aforementioned damage types, the in-service defects, especially the impact-induced damage, and the operation-related damage are of special interest, which can be

categorized as delamination, fiber/matrix cracking, voids, and notch. Many researchers have paid attention to the numerical modelling, experimental testing, and damage detection of the impact related damage. An integrated numerical model for guided-wave structural interrogation was proposed by Zhang et al. [16]. The modelling and assessment of low-velocity impact also aroused much interest [17, 18]. Eddy current pulsed thermography [10], electromagnetic method [19], infrared thermography [20] were put into the application of impact damage monitoring. Apart from the above methods, linear and nonlinear techniques employing the ultrasonic guided waves turn out to be suitable choices due to their long-distance propagation ability and the excellent sensitivity to the presence of structural damage. Various damage types may either result in a degradation of local material properties or induce interfaces with Contact Acoustic Nonlinearity (CAN) [21-23]. The material degradation can be mirrored into the change of typical features related to ultrasonic guided waves [16, 24], such as delay in time-of-flight (ToF), wave reflection and transmission, energy dissipation, and mode conversion. The electromechanical impedance spectroscopy method, due to its high sensitivity to local damage, has also been put into prevailing applications [25-28]. Furthermore, for the detection of the incipient delamination, nonlinear ultrasonic techniques have displayed predominant prowess [29-31], which utilize nonlinear features such as the higher harmonic and wave modulation components as an indication of the CAN phenomena. However, there exist inherent limitations on the aforementioned methods in that (1) they usually aim at detecting a certain damage type, while their sensitivity to other damage types may not be satisfactory; (2) they require at least two or more transducers (forming pitch-catch mode or sensor array), while stand-alone transducer interrogation possesses great advantage of achieving structural diagnosis using a minimum number of sensors; (3) they need a signal of the intact structure as a baseline, while such a baseline may not be available or fluctuate due to environmental variations; (4) they separate linear and nonlinear analysis, while a comprehensive consideration over both domains would provide a more reliable and sensitive structural assessment.

To circumvent the above deficiencies, the paper proposes a nonlinear electromechanical impedance spectroscopy (NEMIS) for the comprehensive monitoring of the CFRC laminates. Different from the conventional EMIS implemented in the frequency domain, the proposed NEMIS with two phases utilizes a temporal chirp interrogative signal to conduct both the linear (Phase I) and nonlinear (Phase II) analysis. The linear part establishes a temporal chirp-based impedance spectrum for the detection of macroscopic damage like voids and fiber/matrix cracks in CFRC laminates. The obtained spectrum is equivalent to that from the conventional EMIS but more time-efficient. Meanwhile, the NEMIS Phase II derives an expanded nonlinear impedance spectrum for the monitoring of incipient damage like delamination. The spectrum can simultaneously capture the resonance information and nonlinear features including the higher harmonics and the wave modulation components.

This paper starts with the comparative illustration of the mechanism and procedures of the conventional EMIS and the proposed NEMIS. Various damage types of CFRC laminates are introduced and classified, followed by the damage mechanism discussion. A general Finite Element Model (FEM) of CFRC laminates is established to verify the feasibility of the NEMIS method. Phase I is applied to detect the macro-scale damage modeled by material properties change. Subsequently, the capability of the NEMIS Phase II capturing nonlinear ultrasonic features is demonstrated.

2. COMPARATIVE ILLUSTRATION OF MECHANISM BEHIND NEMIS

The comparative illustration of the mechanism behind the conventional EMIS and NEMIS is presented in Figure 1. The conventional EMIS takes a frequency domain measurement using a stepwise sweeping excitation. It excites the system with a sinusoid signal at a certain frequency and captures the steady-state response, from which a single impedance value can be calculated. By repeating this procedure from a low frequency to high frequency, the impedance spectrum can be obtained by composing the steady-state response at each step, as shown in Figure 1(a).

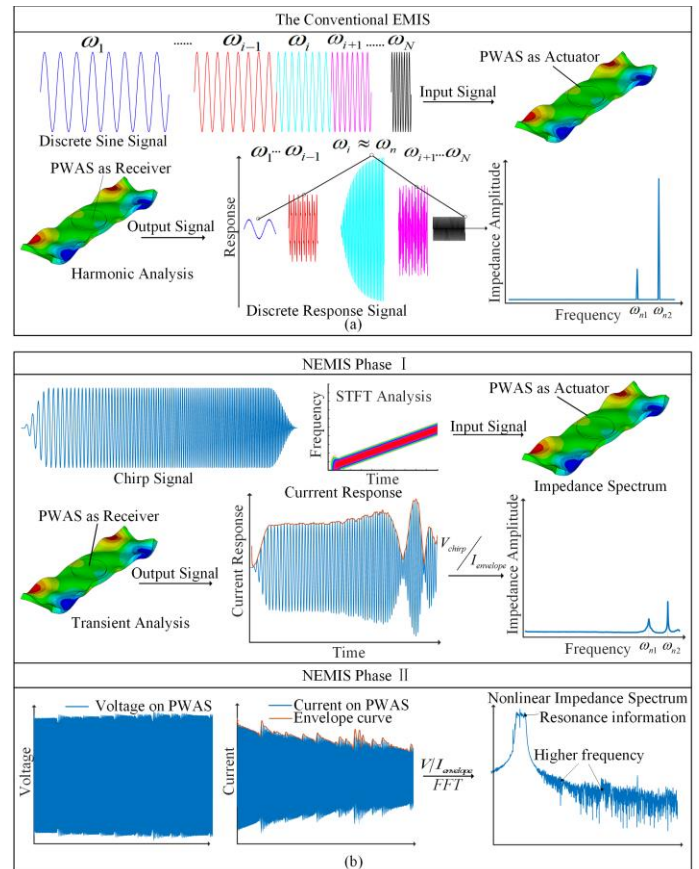


FIGURE 1: THE MECHANISM AND PROCEDURES OF (A) THE CONVENTIONAL EMIS; (B) THE TWO PHASES OF NEMIS.

Regarding the NEMIS Phase I, the single Piezoelectric Wafer Active Sensor (PWAS), functioning as both the actuator and the receiver, is excited by a chirp voltage signal. After obtaining the envelope curve of the electrical current response, the chirp-based impedance spectrum can be derived by dividing the voltage amplitude over the current amplitude. The advanced function of NEMIS is developed in Phase II. Employing the temporal voltage response and the amplitude of current response via $V/I_{envelope}$, and then applying Fast Fourier Transform (FFT), the expanded nonlinear impedance spectrum can be obtained. It contains rich structural information, including the resonance information provided by the fundamental frequency band of the chirp excitation and the nonlinear ultrasonic features. Therefore, it is a combination of the harmonic analysis and the nonlinear ultrasonic techniques.

Regarding the specific implementation of the NEMIS Phase I in an FEM procedure, the transient electrical charge at the multi-physics elements is obtained first. According to the relationship $I = dQ/dt$, the current flowing through the electrode can be calculated, the amplitude of which is captured by an envelope curve. Applying the equation $R = V_{chirp}/I_{envelope}$, where V is a constant excitation voltage amplitude, the chirp-based impedance spectrum can be finally obtained (displayed in last plot in Figure 1(b)).

In summary, the NEMIS technique utilizes continuous temporal excitation with rich time-historical information, which enables the triggering of nonlinear dynamics, the measurement of time-frequency responses, and the extraction of nonlinear features. On the other hand, the conventional EMIS method does not include the transient nonlinear dynamic behavior by merely measuring the steady-state response with amplitude and phase information. Thus, the NEMIS technique pushes the barrier of impedance methods to include and distinguish nonlinear components.

3. DAMAGE TYPES AND MECHANISM IN CARBON FIBER REINFORCED LAMINATES

Carbon fiber reinforced composites are susceptible to various damage scenarios, with manufacturing, handling and installation, and in-service usage being three major sources. Manufacturing defects, including fiber waviness, poor interface adhesion, voids, etc., may cause a reduction of the local material properties and become a potential damage initiation origin while bearing external loadings. Meanwhile, unexpected impacts, inappropriate drilling, and incorrect exposure to adverse environments can lead to a reduced fatigue tolerance and a tremendous reduction in mechanical properties. In-service damage is the most universal cause for structural integrity degradation, resulting from the environmental influences, impacts, cyclic or static loadings.

The damage mechanisms of carbon fiber reinforced composites can be classified into five types: delamination, fiber breakage, matrix cracking, fiber-matrix debonding, and void. Delamination occurs at the ply interfaces of CFRC laminates under most loading conditions like tensile and compression

fatigue loading and impact loading. It can impose a significant influence on the tensile and compression strength of CFRC, resulting in a severe mechanical performance reduction despite a small delamination size. The fibers play a dominant role in sustaining external loads in CFRCs, whose breakage may lead to considerable reduction in strength and stiffness. Even tiny fiber fractures could result in catastrophic failures of structures. Matrix cracking denotes the material splits in the polymer matrix. Furthermore, the occurrence of debondings between the carbon fiber and the polymer matrix happens when the shear stress from flexural loading or bending exceeds the bonding strength. Voids belong to manufacturing defects in CFRC, especially those which are not autoclaved but are produced by predominantly hand-lay-up process, during which voids can be generated via air entrapment. The first 1% of voids can cause severe material properties degradation, such as flexural strength (30% reduction), tensile strength (3% decrement), and impact strength (8% decrease). The schematic diagram of various damage types is displayed below in Figure 2.

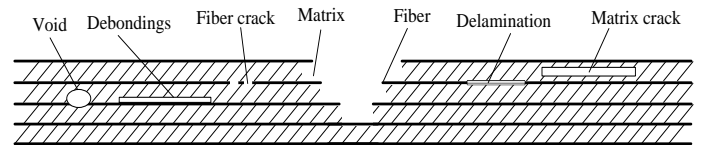


FIGURE 2: THE MECHANISM OF VARIOUS DAMAGE TYPES IN CFRC LAMINATES.

4. ILLUMINATION OF STRUCTURAL NONLINEAR DYNAMIC RESPONSE USING A 1-D CAN MODEL

CAN is derived from the contact dynamic behavior of interfaces experiencing periodic collisions, resulting in the change of local structural stiffness. The incipient damage in CFRC laminates like the delamination can be modeled by CAN. Wang et al. proposed a nonlinear oscillator model with a transitional region to capture the rough crack surfaces, which approximates the practical situation [21]. Based on the model showcased in Figure 3(a), numerical studies were conducted using the central difference computation method to capture the chirp-induced nonlinear ultrasonic phenomena, including the higher harmonics and nonlinear wave modulation.

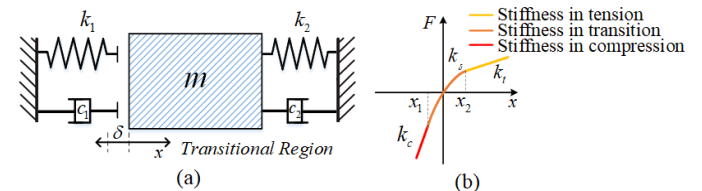


FIGURE 3: (A) THE BILINEAR CAN MODEL WITH A TRANSITIONAL REGION; (B) THE LOCAL STIFFNESS CURVE OF THE MODEL.

For this bilinear CAN model, the equation of motion takes the form of

$$m\ddot{u}(t) + c(u)\dot{u}(t) + k(u)u(t) = p(t) \quad (1)$$

where m denotes the mass of oscillator; $u(t)$ signifies the displacement; $c(u)$ and $k(u)$ represent the displacement-dependent damping coefficients and the stiffness; $p(t)$ refers to the external loading. When the crack is open, the stiffness $k = k_1 = k_2$. When the crack is closed, the stiffness $k = k_c = k_1 + k_2$. When the crack is in the transitional region, the value of the stiffness follows a polynomial form [32].

$$k_{eff} = \beta + \beta_1 x + \beta_2 x^2 + \beta_3 x^3 + \beta_4 x^4 + \beta_5 x^5 + \dots + \beta_n x^n \quad (2)$$

The overall expression for the stiffness can be formulated as

$$k(u_i) = \begin{cases} k_c = k_1 + k_2, & u_i \leq x_1 \\ \beta + \beta_1 u_i + \beta_2 u_i^2 + \beta_3 u_i^3 + \beta_4 u_i^4 + \beta_5 u_i^5, & x_1 \leq u_i \leq x_2 \\ k_1 = k_2, & x_2 \leq u_i \end{cases} \quad (3)$$

where u_i represents the displacement response at i -th time step through the time marching procedure.

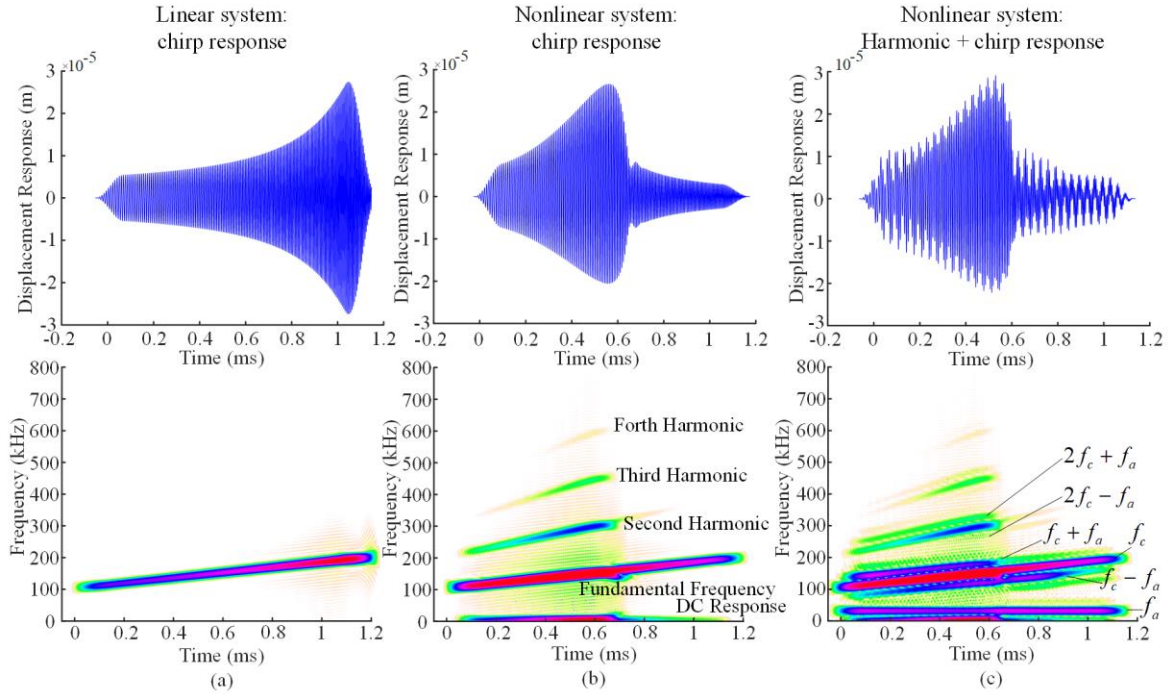


FIGURE 4: THE TRANSIENT DISPLACEMENT RESPONSE AND THE CORRESPONDING SHORT TIME FOURIER TRANSFORM (STFT) RESULT OF (A) THE LINEAR SYSTEM; (B) THE NONLINEAR SYSTEM WITH PURE CHIRP EXCITATION; (C) THE NONLINEAR SYSTEM WITH MIXED CHIRP EXCITATION.

To capture the nonlinear ultrasonic phenomena, two kinds of excitation signals were applied. The first one was a pure chirp signal with the frequency from 100 kHz to 200 kHz, while the second was the same chirp signal mixed with a 30 kHz sinusoidal waveform. Setting up the corresponding parameters and then applying the central difference method, the temporal response of the system and the corresponding Short Time Fourier Transform (STFT) results were obtained in Figure 4. For the linear system shown in Figure 4(a), the frequency components of the output response are consistent with those of the input signal, 100-200 kHz. Regarding the higher harmonic components resulting from the CAN, second harmonic (200-400 kHz), third harmonic (300-600 kHz), and fourth harmonic (400-800 kHz) are generated and clearly observed in Figure 4(b). As for the wave modulation

phenomenon, the low frequency sine signal interacts with the chirp signal, rendering several side bands as marked in Figure 4(c). Not only the fundamental frequency band (100-200 kHz) is modulated by the sine wave but also the higher harmonic frequency bands as well. The numerical analysis demonstrates the feasibility of employing a chirp signal to conduct the nonlinear ultrasonic inspection for the detection of delamination.

5. FEM SIMULATION OF NEMIS FOR COMPREHENSIVE DAMAGE DETECTION

In this section, FEM simulation was carried out to demonstrate the NEMIS for the monitoring of the CFRC laminates. According to the aforementioned damage mechanism, most damage types of CFRC, such as fiber injuries (including

fiber distortion, fiber breakage, and fiber crack), voids, and matrix cracking, can lead to the degradation of the mechanical properties. Meanwhile, the delamination occurring at the ply interfaces of the CFRC laminates can be simulated by setting up contact pairs. Therefore, in the simulation part, a general CFRC beam model was established as showcased in Figure 5.

5.1 Finite Element model layout and parameter settings

As for the CFRC laminates FEM model displayed in Figure 5, it stands as an example, which may represent a general structure. The model was composed of six layers with the $[0/90]_3$ arrangement and the stiffness matrix with Voigt Notation was displayed in Table 1. A damage region was established as marked with the red lines. The damage types, such as fiber defects and voids were modeled by the material property changes of the stiffness matrix and the density. Damage types like the delamination and debondings were implemented by the contact elements to simulate opening and closing motions of the interlaminates.

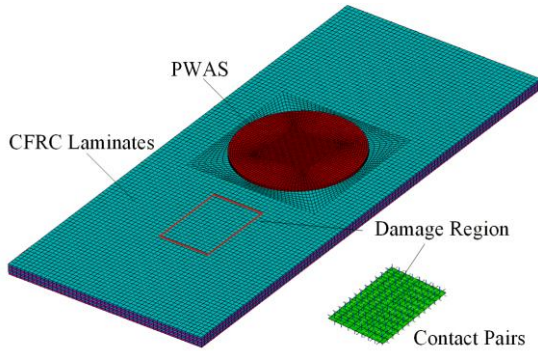


FIGURE 5: FEM MODEL OF CFRC LAMINATES WITH A DELAMINATION REGION.

TABLE 1: STIFFNESS MATRIX OF THE CFRC MATERIAL FOR 0° ARRANGEMENT.

C_{11} 1.69E11	C_{12} 0.067E11	C_{13} 0.067E11
C_{22} 0.155E11	C_{23} 0.067E11	C_{33} 0.067E11
C_{44} 0.044E11	C_{55} 0.046E11	C_{66} 0.046E11

5.2 The Linear aspect: baseline EMIS results

For the macro-scale damage types, three cases were set with 5%, 10%, and 15% degradation of the material properties. NEMIS Phase I was adopted to conduct the damage detection, which utilizes the chirp-based impedance spectra with the resonance information. The implementation procedures were illuminated in Figure 1(b) and the chirp-based impedance spectra were showcased in Figure 6(a).

It can be observed that there were two resonant peaks from 336 kHz to 346 kHz for each case. Particularly, the locations of the resonant peaks for the pristine case were 340.4 kHz and 345.1 kHz. With the decrement of the overall material properties, the resonant peaks displayed a leftward and downward deviation. The deviation trends were in good consistency with the increasing degradation of the material properties. Specifically,

the location of the first resonant peak deviated from 340.4 kHz to 339.9 kHz, to 339.3 kHz, and finally to 338.7 kHz, with the impedance amplitude value from 2.198×10^{10} Ohms to 1.381×10^{10} Ohms, to 6.695×10^9 Ohms, and ultimately to 3.419×10^9 Ohms, corresponding to the pristine, -5%, -10%, and -15% material degradation respectively. To further quantify the severity of the damage by evaluating the deviation degree of the two resonant peaks, the damage index, Root Mean Square Deviation (RMSD), was applied, the formulation of which was listed below. It can be concluded from the RMSD curve in Figure 6(b) that, the RMSD value underwent a monotonic increment with the development of the damage severity.

$$\text{RMSD} = \sqrt{\frac{\sum_N [R_i - R_0]^2}{\sum_N [R_0]^2}} \quad (4)$$

where R_i represents the impedance for each case while R_0 denotes the pristine case.

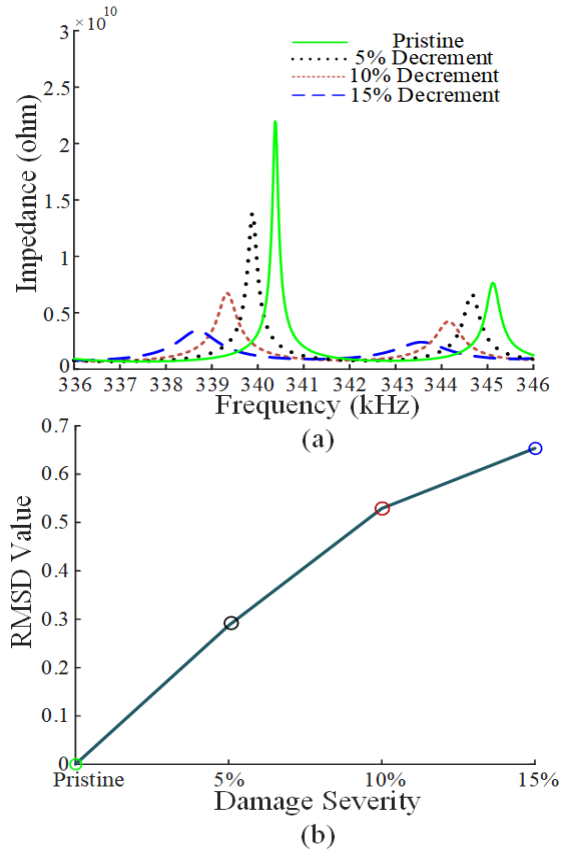


FIGURE 6: (A) THE CHIRP-BASED IMPEDANCE SPECTRA FOR DAMAGE CASES OF MATERIAL PROPERTIES DEGRADATION; (B) THE RMSD CURVE FOR DIFFERENT DAMAGE SEVERITIES.

5.3 The nonlinear aspect: baseline-free NEMIS results

After applying NEMIS Phase I for the detection of damage modeled by material properties change, NEMIS Phase II was

employed to monitor the existence of the laminates delamination, followed by the quantification of damage severity without referring to the pristine baseline signal. Different sizes and layers of delamination region were set with the contact elements to simulate different severities of the damage as displayed in Figure 7.

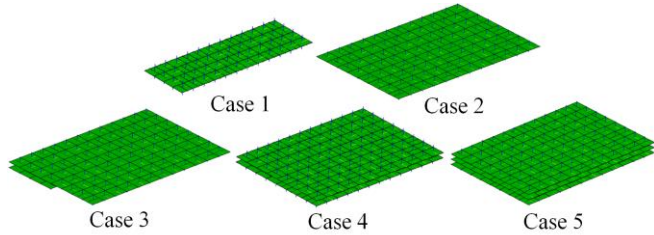


FIGURE 7: ILLUSTRATION OF DELAMINATION REGIONS OF DIFFERENT SEVERITIES.

It is worth mentioning that the NEMIS applied in the FEM simulation is not the ultimate version but the simplified one. Since the instantaneous temporal voltage response at the PWAS terminal cannot be captured, the impedance value is unavailable. Consequently, to demonstrate the NEMIS methodology capturing the nonlinear frequency components, the electrical current response was obtained for the nonlinear spectral analysis via the electrical charge variation at PWAS terminals. The simplification in the FEM analysis was reasonable because the frequency components of the current response were identical to the proposed temporal impedance spectra shown in Figure 1(b) with only the difference in the absolute amplitude.

Exciting the PWAS with a chirp voltage signal sweeping from 300 kHz to 350 kHz lasting for 0.3 ms, after the corresponding signal processing, the relative nonlinear ultrasonic impedance spectra were derived in Figure 8. It could be observed that each nonlinear impedance spectra could generate a smooth curve, depicting the overall trend of the spectrum. The smooth inherent curve was called chaos-defused baseline and was obtained by exerting a wave filter on the original spectrum. It was developed to play the role of an instantaneous baseline without referring to the pristine curve for the quantification of delamination severity. The nonlinearity of the system could be quantified by evaluating the chaos level of

the nonlinear impedance spectra at a certain frequency band. Specifically, for the chirp excitation sweeping from 300 kHz to 350 kHz, the higher harmonic frequency components including the second harmonic (600-700kHz) and the third harmonic (900-1050 kHz) should be paid attention to. That is to say, if the spectra vibrate more violently against the chaos-defused baseline in these frequency bands, the delamination would be more severe. Apart from the higher harmonics, another typical nonlinear feature, the wave modulation, could also be observed due to the rich frequency components of the chirp excitation. Taking case 5 as an example, when the delamination region and layers became larger, wave modulation could be captured between the second harmonics and the third harmonics (600 kHz –1050 kHz) and over even a much higher frequency band (>1050 kHz).

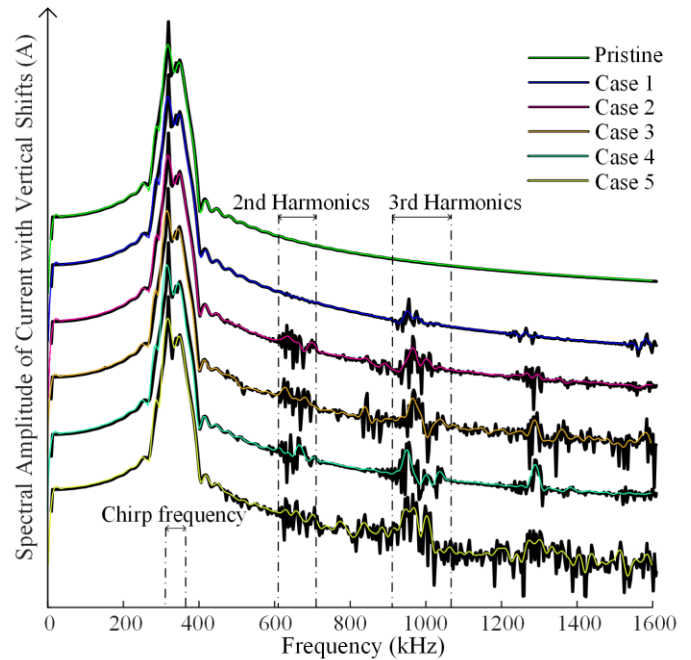


FIGURE 8: NONLINEAR ULTRASONIC SPECTRA WITH CHAOS-DEFUSED BASELINE FOR DIFFERENT CASES.

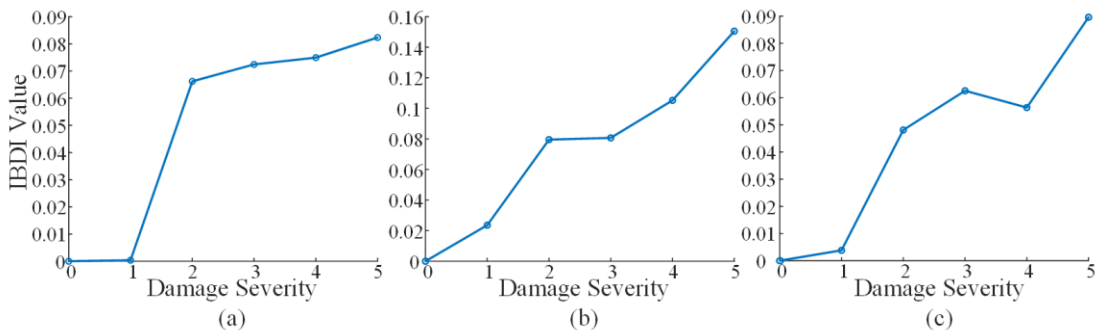


FIGURE 9: INSTANTANEOUS BASELINE DEVIATION INDEX (IBDI) VALUE FOR (A) THE SECOND HARMONICS (600 KHZ-700 KHZ); (B) THE THIRD HARMONICS (900 KHZ-1050 KHZ); (C) COMPREHENSIVE FREQUENCY BAND (600 KHZ-1050 KHZ).

To quantify the delamination severity, a nonlinear parameter, Instantaneous Baseline Deviation Index (IBDI), was developed, which was formulated as

$$IBDI = \frac{\sum_{i(f_1)}^{i(f_2)} (P_i - P_0)^2}{\sum_{i(f_1)}^{i(f_2)} P_0^2} \quad (5)$$

where P_i signifies the spectral amplitude of the FFT result of the current signal while P_0 denotes the pristine case.

IBDI was applied in the second harmonic (600 kHz-700 kHz), third harmonic frequency (900 kHz-1050 kHz) band, and a comprehensive frequency band (600 kHz-1050 kHz) including not only the higher harmonics but also the wave modulation components, as displayed in Figure 9. Generally, with the growth of the delamination severity, the IBDI value presented an upward growing trend. It could be observed that the IBDI of the second harmonic components for Case 1 was almost zero, while the IBDI value of third harmonic component showed obvious increment. It is apparent that different frequency band harmonic responses did not possess the same sensitivity to the same damage severity. Thus, the simplified NEMIS Phase II demonstrated its capability to detect the existence and quantify the severity of the delamination. The successful implementation of the simplified NEMIS in FEM analysis offers the foundation and guidance for the further investigation of NEMIS in experimental and practical settings.

6. CONCLUDING REMARKS AND FUTURE WORK

This paper presented a Nonlinear Electromechanical Impedance Spectroscopy (NEMIS) for the comprehensive monitoring of CFRC laminates. It was found that NEMIS stood as an efficient and multifunctional method according to the illustration of the conventional EMIS and NEMIS mechanisms. Various damage types of the CFRC laminates were introduced, bringing about the difficulty and complexity for the damage detection in CFRCs. Subsequently, numerical studies on the 1-D CAN model and 3-D FEM analysis were carried out. The chirp-induced nonlinear features utilizing higher harmonics and wave modulation were illuminated by the CAN model. Besides, both macro and micro scale damage types could be successfully detected and quantified by the linear and nonlinear information from the two phases of NEMIS. It was found that both the linear RMSD value and the nonlinear IBDI value conformed with a monotonically changing trend for the growing damage severity. It could be concluded that NEMIS could serve as an effective and comprehensive methodology for the SHM of CFRC structures.

The future work will be focused on the experimental demonstration of the NEMIS for the practical monitoring of the CFRC laminates.

7. ACKNOWLEDGEMENTS

The support from the National Natural Science Foundation of China (contract numbers 51975357 and 51605284) is thankfully acknowledged; this research is also sponsored by the Shanghai Rising-star Program (contract number 21QA1405100).

REFERENCES

- [1] P. Ghatage, V. Kar, and E. Sudhagar, "On the numerical modelling and analysis of multi-directional functionally graded composite structures: A review," *Composite Structures*, vol. 236, p. 111837, 03/01 2020, doi: 10.1016/j.compstruct.2019.111837.
- [2] A. Güemes, A. Fernandez-Lopez, A. R. Pozo, and J. Sierra-Pérez, "Structural Health Monitoring for Advanced Composite Structures: A Review," *Journal of Composites Science*, vol. 4, no. 1, 2020, doi: 10.3390/jcs4010013.
- [3] W. Nsengiyumva, S. Zhong, J. Lin, Q. Zhang, J. Zhong, and Y. Huang, "Advances, limitations and prospects of nondestructive testing and evaluation of thick composites and sandwich structures: A state-of-the-art review," *Composite Structures*, vol. 256, p. 112951, 01/15 2021, doi: 10.1016/j.compstruct.2020.112951.
- [4] S. Hassani, M. Mousavi, and A. H. Gandomi, "Structural Health Monitoring in Composite Structures: A Comprehensive Review," *Sensors (Basel)*, vol. 22, no. 1, Dec 27 2021, doi: 10.3390/s22010153.
- [5] W. Fan and P. Qiao, "Vibration-based Damage Identification Methods: A Review and Comparative Study," *Structural Health Monitoring-an International Journal - STRUCT HEALTH MONIT*, vol. 9, 02/02 2010, doi: 10.1177/1475921710365419.
- [6] M. Thor, M. G. R. Sause, and R. M. Hinterhölzl, "Mechanisms of Origin and Classification of Out-of-Plane Fiber Waviness in Composite Materials—A Review," *Journal of Composites Science*, vol. 4, no. 3, 2020, doi: 10.3390/jcs4030130.
- [7] M. Mehdikhani, L. Gorbatiikh, I. Verpoest, and S. V. Lomov, "Voids in fiber-reinforced polymer composites: A review on their formation, characteristics, and effects on mechanical performance," *Journal of Composite Materials*, vol. 53, no. 12, pp. 1579-1669, 2019/05/01 2018, doi: 10.1177/0021998318772152.
- [8] M. Nebe, T. Schmack, T. Schaefer, and F. Walther, "Experimental and numerical investigation on the impact response of CFRP under 3-point-bending," *Composites Part C: Open Access*, vol. 4, 2021, doi: 10.1016/j.jcomc.2020.100079.
- [9] C. Hu, G. Huang, and C. Li, "Experimental and Numerical Study of Low-Velocity Impact and Tensile after Impact for CFRP Laminates Single-Lap Joints Adhesively Bonded Structure," *Materials (Basel)*, vol. 14, no. 4, Feb 21 2021, doi: 10.3390/ma14041016.

- [10] Y. He, G. Tian, M. Pan, and D. Chen, "Impact evaluation in carbon fiber reinforced plastic (CFRP) laminates using eddy current pulsed thermography," *Composite Structures*, vol. 109, pp. 1-7, 2014, doi: 10.1016/j.compstruct.2013.10.049.
- [11] G. Ding, W. Song, X. Gao, H. Cao, and J. Yang, "Damage Detection in Holed Carbon Fiber Composite Laminates Using Embedded Fiber Bragg Grating Sensors Based on Strain Information," *Shock and Vibration*, vol. 2020, pp. 1-11, 2020, doi: 10.1155/2020/8813213.
- [12] D. Geng *et al.*, "Delamination formation, evaluation and suppression during drilling of composite laminates: A review," *Composite Structures*, vol. 216, pp. 168-186, 2019, doi: 10.1016/j.compstruct.2019.02.099.
- [13] Z. Jia, T. Li, F.-p. Chiang, and L. Wang, "An experimental investigation of the temperature effect on the mechanics of carbon fiber reinforced polymer composites," *Composites Science and Technology*, vol. 154, pp. 53-63, 2018/01/18/ 2018, doi: 10.1016/j.compscitech.2017.11.015.
- [14] X. F. Wan, Y. L. Wang, F. G. Zhou, and Y. Z. Wan, "Moisture Absorption Behavior of Carbon Fiber-Reinforced Monomer Casting Nylon Composites," *Journal of Reinforced Plastics and Composites*, vol. 23, no. 10, pp. 1031-1040, 2004/07/01 2004, doi: 10.1177/0731684404033961.
- [15] T. Yokozeki, Y. Iwahori, and S. Ishiwata, "Matrix cracking behaviors in carbon fiber/epoxy laminates filled with cup-stacked carbon nanotubes (CSCNTs)," *Composites Part A: Applied Science and Manufacturing*, vol. 38, no. 3, pp. 917-924, 2007/03/01/ 2007, doi: 10.1016/j.compositesa.2006.07.005.
- [16] B. Zhang *et al.*, "An integrated numerical model for investigating guided waves in impact-damaged composite laminates," *Composite Structures*, vol. 176, pp. 945-960, 2017, doi: 10.1016/j.compstruct.2017.06.034.
- [17] Y. Shi and C. Soutis, "Modelling low velocity impact induced damage in composite laminates," *Mechanics of Advanced Materials and Modern Processes*, vol. 3, no. 1, p. 14, 2017/07/26 2017, doi: 10.1186/s40759-017-0029-x.
- [18] E.-H. Kim, M.-S. Rim, I. Lee, and T.-K. Hwang, "Composite damage model based on continuum damage mechanics and low velocity impact analysis of composite plates," *Composite Structures*, vol. 95, pp. 123-134, 2013, doi: 10.1016/j.compstruct.2012.07.002.
- [19] Z. Li *et al.*, "Detection of Impact Damage in Carbon Fiber Composites Using an Electromagnetic Sensor," *Research in Nondestructive Evaluation*, vol. 29, no. 3, pp. 123-142, 2018/07/03 2018, doi: 10.1080/09349847.2016.1263772.
- [20] C. Meola, G. Carlomagno, and F. Ricci, *Monitoring of impact damage in Carbon Fibre Reinforced Polymers*. 2012.
- [21] J. Wang, Y. Shen, R. Danyu, and W. Xu, "An instantaneous-baseline multi-indicial nonlinear ultrasonic resonance spectral correlation technique for fatigue crack detection and quantification," *Nonlinear Dynamics*, vol. 103, 01/01 2021, doi: 10.1007/s11071-020-06128-x.
- [22] J. Wang, Y. Shen, D. Rao, and W. Xu, "Physical-virtual time reversing of nonlinear Lamb waves for fatigue crack detection and quantification," *Mechanical Systems and Signal Processing*, vol. 160, p. 107921, 2021/11/01/ 2021, doi: 10.1016/j.ymssp.2021.107921.
- [23] Y. Shen and C. E. S. Cesnik, "Nonlinear scattering and mode conversion of Lamb waves at breathing cracks: An efficient numerical approach," *Ultrasonics*, vol. 94, pp. 202-217, 2019/04/01/ 2019, doi: 10.1016/j.ultras.2018.09.011.
- [24] K. Diamanti, J. M. Hodgkinson, and C. Soutis, "Detection of Low-velocity Impact Damage in Composite Plates using Lamb Waves," *Structural Health Monitoring*, vol. 3, no. 1, pp. 33-41, 2016, doi: 10.1177/1475921704041869.
- [25] M. Gresil and V. Giurgiutiu, "Electromechanical Impedance Spectroscopy and Guided Wave Propagation Predictive Modeling on Composite Materials," presented at the EWSHM - 7th European Workshop on Structural Health Monitoring, Nantes, France, 2014, 2014.
- [26] T. Wandowski, P. Malinowski, L. Skarbek, and W. Ostachowicz, "Moisture detection in carbon fiber reinforced polymer composites using electromechanical impedance technique," *Proceedings of the Institution of Mechanical Engineers, Part C: Journal of Mechanical Engineering Science*, vol. 230, no. 2, pp. 331-336, 2015, doi: 10.1177/0954406215574239.
- [27] P. Selva, O. Cherrier, V. Budinger, F. Lachaud, and J. Morlier, "Smart monitoring of aeronautical composites plates based on electromechanical impedance measurements and artificial neural networks," *Engineering Structures*, vol. 56, pp. 794-804, 2013, doi: 10.1016/j.engstruct.2013.05.025.
- [28] R. Lu and Y. Shen, "High-Damping Viscoelastic Material Monitoring Using Sub-Resonator Enhanced Electro-Mechanical Impedance Spectroscopy," in *ASME 2021 International Mechanical Engineering Congress and Exposition*, 2021, vol. Volume 1: Acoustics, Vibration, and Phononics, V001T01A011, doi: 10.1115/imece2021-71172. [Online]. Available: <https://doi.org/10.1115/IMECE2021-71172>
- [29] C. Andreades, M. Meo, and F. Ciampa, "Tensile and fatigue testing of impacted smart CFRP composites with embedded PZT transducers for nonlinear

- ultrasonic monitoring of damage evolution," *Smart Materials and Structures*, vol. 29, no. 5, 2020, doi: 10.1088/1361-665X/ab7f41.
- [30] F. Aymerich and W. J. Staszewski, "Impact damage detection in composite laminates using nonlinear acoustics," *Composites Part A: Applied Science and Manufacturing*, vol. 41, no. 9, pp. 1084-1092, 2010/09/01/ 2010, doi: <https://doi.org/10.1016/j.compositesa.2009.09.004>.
- [31] U. Polimeno, M. Meo, D. P. Almond, and S. Angioni, "Detecting Low Velocity Impact Damage in Composite Plate Using Nonlinear Acoustic/Ultrasonic Methods," *Applied Composite Materials*, vol. 17, pp. 481-488, 10/01 2010, doi: 10.1007/s10443-010-9168-5.
- [32] K. Jhang, "Nonlinear ultrasonic techniques for non destructive assessment of micro damage in materials: A review," *International Journal of Precision Engineering and Manufacturing*, vol. 10, pp. 123-135, 2009, doi: 10.1007/S12541-009-0019-Y.